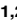




RESEARCH ARTICLE

Modelling the Stoichiometric Regulation of C-Rich Toxins in Marine Dinoflagellates

Adriano Pinna^{1,2}, Laura Pezzolesi¹, Rossella Pistocchi¹, Silvana Vanucci³, Stefano Ciavatta^{2,4}, Luca Polimene^{2*}

1 Department of Biological, Geological and Environmental Sciences (BiGeA)—University of Bologna, Via Sant'Alberto 163, 48123 Ravenna, Italy, **2** Plymouth Marine Laboratory, Prospect Place, The Hoe, PL1 3DH Plymouth, United Kingdom, **3** Department of Biological and Environmental Sciences—University of Messina, Viale Ferdinando d'Alcontres 31, 98166 S. Agata, Messina, Italy, **4** National Centre for Earth Observation (NCEO), Plymouth Marine Laboratory, Plymouth, United Kingdom

 These authors contributed equally to this work.

* luca@pml.ac.uk



CrossMark
click for updates

OPEN ACCESS

Citation: Pinna A, Pezzolesi L, Pistocchi R, Vanucci S, Ciavatta S, Polimene L (2015) Modelling the Stoichiometric Regulation of C-Rich Toxins in Marine Dinoflagellates. PLoS ONE 10(9): e0139046. doi:10.1371/journal.pone.0139046

Editor: Hans G. Dam, University of Connecticut, UNITED STATES

Received: March 12, 2015

Accepted: September 7, 2015

Published: September 23, 2015

Copyright: © 2015 Pinna et al. This is an open access article distributed under the terms of the [Creative Commons Attribution License](http://creativecommons.org/licenses/by/4.0/), which permits unrestricted use, distribution, and reproduction in any medium, provided the original author and source are credited.

Data Availability Statement: All relevant data are within the paper and its Supporting Information files.

Funding: Luca Polimene was funded through the UK Natural Environment Research Council (NERC, www.nerc.ac.uk) National Capability in sustained observations and marine modelling. Stefano Ciavatta was partly funded through the UK Natural Environment Research Council (NERC) National centre for Earth Observation (NCEO). Laura Pezzolesi, Rossella Pistocchi and Adriano Pinna were funded by the Italian Ministero dell'Istruzione, dell'Università e della Ricerca (MIUR, www.istruzione.it), through the "Progetti di Ricerca di Interesse

Abstract

Toxin production in marine microalgae was previously shown to be tightly coupled with cellular stoichiometry. The highest values of cellular toxin are in fact mainly associated with a high carbon to nutrient cellular ratio. In particular, the cellular accumulation of C-rich toxins (i.e., with C:N > 6.6) can be stimulated by both N and P deficiency. Dinoflagellates are the main producers of C-rich toxins and may represent a serious threat for human health and the marine ecosystem. As such, the development of a numerical model able to predict how toxin production is stimulated by nutrient supply/deficiency is of primary utility for both scientific and management purposes. In this work we have developed a mechanistic model describing the stoichiometric regulation of C-rich toxins in marine dinoflagellates. To this purpose, a new formulation describing toxin production and fate was embedded in the European Regional Seas Ecosystem Model (ERSEM), here simplified to describe a monospecific batch culture. Toxin production was assumed to be composed by two distinct additive terms; the first is a constant fraction of algal production and is assumed to take place at any physiological conditions. The second term is assumed to be dependent on algal biomass and to be stimulated by internal nutrient deficiency. By using these assumptions, the model reproduced the concentrations and temporal evolution of toxins observed in cultures of *Ostreopsis cf. ovata*, a benthic/epiphytic dinoflagellate producing C-rich toxins named ova-toxins. The analysis of simulations and their comparison with experimental data provided a conceptual model linking toxin production and nutritional status in this species. The model was also qualitatively validated by using independent literature data, and the results indicate that our formulation can be also used to simulate toxin dynamics in other dinoflagellates. Our model represents an important step towards the simulation and prediction of marine algal toxicity.

nazionale (PRIN) 2009, Rome, Italy. The funders had no role in study design, data collection and analysis, decision to publish, or preparation of the manuscript.

Competing Interests: The authors have declared that no competing interests exist.

Introduction

Blooms of toxic microalgae are increasing worldwide and their proliferation seems to be driven by several environmental and anthropogenic factors. Among these the supply of nutrients (N and P) to surface waters are of particular importance [1,2,3]. Algal toxins are highly diverse in chemical structure (ranging from N-rich alkaloids to C-based polyketides), molecular weight and mechanism of action. Van de Waal et al. [4] subdivided phytoplanktonic toxins into two main families, 1) N-rich and 2) C-rich toxins (C:N molar ratio <6.6 and >6.6 , respectively), and showed that the synthesis of both groups is highly coupled to cellular stoichiometry (given as the N:P ratio). However, while N-rich toxins are stimulated only by P-limitation (and are repressed under N-limitation), C-rich toxins are stimulated by both N and P-limitation. More specifically, the content of N-rich toxins seems to be linearly correlated with the cellular N:P ratio, while for C-rich toxins the dynamics are more complicated and N:P stoichiometry alone is not sufficient for interpreting and predicting toxin dynamics [4]. This is probably due to the fact that C-rich toxins are more sensitive to several environmental factors (e.g. light, CO_2) in addition to the limiting nutrients [2].

Under unbalanced growth conditions (e.g. under increasing C:P), the production of C-rich toxin has been interpreted as a way to store excess carbon in secondary pools [4] and/or secondary metabolites which can act as defense against grazers. The latter mechanism is also known as the carbon to nutrient balance hypothesis or CNBH [5].

Among the organisms producing C-rich toxins, *Ostreopsis cf. ovata* Fukuyo represents an increasing issue throughout the world, particularly in temperate areas. This microalga produces different palytoxin (PLTX)-like compounds, namely the recently re-named isobaric-PLTX (previously known as putative-PLTX) and seven analogues named ovatoxins (OVTXs): OVTX-a, -b, -c, -d/e, -f, -g [6,7,8]. When the density of this dinoflagellate in seawater is high (i.e. when it blooms) the extracellular concentration of its toxins may also reach critical levels, inducing respiratory and febrile syndrome outbreaks in humans exposed to seawater and/or marine aerosol [9,10]. These toxins may also enter the food chain and accumulate in different kinds of edible species (from mollusks to fish and crustaceans) causing severe human intoxication [11]. *O. cf. ovata* is known to be dangerous also for the marine environment by inducing severe mass mortalities within benthic communities [12,13,14,15].

Experimental work investigating the role of nutrients in *O. cf. ovata* growth and toxicity gave apparently contrasting results. Vanucci et al. [16] observed decreasing cellular growth and total toxin amount in batch cultures when shifting from balanced N:P conditions (N:P molar ratio of 16 in the culture medium, according to Redfield [17,18]), to P-deficiency (N:P = 92) and to N-deficiency (N:P = 5) conditions. By contrast, Vidyarthna & Granéli [19] observed a significantly higher toxicity (measured as hemolytic activity) in cultures grown in N-limited conditions (N:P = 1.6). Although the decrease in toxin production under nutrient depletion might represent a noteworthy exception to the CNBH, Pezzolesi and colleagues [20] observed a higher ovatoxins production concomitantly with conditions of unbalanced growth and this suggests that the stoichiometric regulation of C-rich toxin discussed in Van de Waal et al. [4] applies also to *O. cf. ovata*.

While the functional linkage between cellular stoichiometry and toxin production is regarded as a general feature of toxic dinoflagellates [4], a numerical model describing this function is still lacking and this limits our capacity to simulate and predict microalgal toxicity.

The objective of this paper is to develop a mechanistic model describing C-rich toxin production in marine dinoflagellates. The model was developed by interpreting the dataset presented in Pezzolesi et al. [20] describing growth and toxin production in *O. cf. ovata*. The choice of this organism has been driven by: 1) its ecological relevance and 2) the availability of

one of the most complete datasets for a toxic dinoflagellate. The dataset used also included unpublished analyses of cellular elemental composition (C:N:P) and bacteria biomass relative to the experiments described in [20]. The new formulation has been embedded in the primary producer module of the European Regional Seas Marine Ecosystem Model (ERSEM) [21], which was simplified to reproduce a mono-specific batch culture. A sub-model describing bacterial dynamics (already present in ERSEM) was also used to mimic the bacterial activity associated with the algal cultures. The model was run by using experimental temperature and light regimes (intensity and light/dark cycle) and actual initial conditions. Model simulations provided a conceptual framework linking cellular nutrient content (given as carbon to nutrient ratio) to growth and toxin production in *O. cf. ovata*. Subsequently, the model was validated against independent literature data to test its applicability to different microalgae producing C-rich toxins ([4] and references therein).

Materials and Methods

Data

Experimental conditions. The numerical model was developed by interpreting the data obtained in the experiment presented in Pezzolesi et al. [20], where a strain of *O. cf. ovata* Fukuyo (OOAB0801) isolated in 2008 in the Western Adriatic Sea during a bloom near Bari (Italy) was used. Experimental batch cultures were prepared by adding macronutrients at a five-fold diluted $f/2$ concentration [22] and selenium to filtered and autoclaved natural seawater (at salinity 36). Triplicate cultures consisted of 3 L Erlenmeyer flasks, inoculated with cells collected from a culture at early stationary phase and fresh medium to a final volume of 2500 mL, maintained under illumination from cool white light at a photon flux density of 110–120 $\mu\text{mol m}^{-2} \text{s}^{-1}$, at $20 \pm 1^\circ\text{C}$ on a 16:8 h light/dark cycle in a growth chamber.

Measurements of carbon and nitrogen in the cells were performed by filtering culture aliquots (10 mL) on GF/F glass-fiber filters (Whatman) precombusted at 550°C for 20 min. Elemental analysis was conducted using a ThermoFisher organic elemental analyzer (Flash 2000) configured for CHNS-O determination using a copper/copper oxide column. The standard 2,5-bis-(5-tert-butyl-2-benzoxazol-2-yl) thiophene (BBOT) was used for calibration. Particulate phosphate was measured photometrically (UV/VIS, JASCO 7800, Tokyo, Japan) after digestion with a solution of 5% potassium peroxide using the method described by [23].

Algal and bacteria carbon. A growth-curve describing the evolution of carbon biomass of *O. cf. Ovata*, was built by using data from CHN analyses (Fig 1). However, it is likely that the particulate organic carbon (POC) detected by the CHN was affected by the presence of the extra-cellular polysaccharidic mucilage, which is copiously produced by *O. cf. ovata* particularly during the stationary phase [24,19,20,25]. This has probably generated the extremely high POC to PON and POC to POP ratios measured at the end of the experiment (up to 25 and 500 for molar C:N and C:P ratios, respectively). The latter values are extremely high if compared to both field [26,27] and laboratory [28,29,30] observations for marine microalgae. To overcome this problem, the last part of the POC curve was corrected by using the regression line describing the correlation ($r > 0.99$; $p < 0.01$, see S1 Fig) between the POC and the total cell volume in the first 15 day of the experiment, when the presence of mucilage was low and so POC was a good estimator of algal carbon. The presence of bacteria and their growth in the algal cultures were assessed by direct bacteria counts using epifluorescence microscopy after staining with SYBR gold [31].

Bacteria biomass was estimated from cell counts and mean cell volumes assuming a carbon content of 145 fg C μm^{-3} [32,33]. Bacterial nitrogen and phosphorus were calculated assuming a fixed C:N:P molar ratio of 45:9:1 [34].

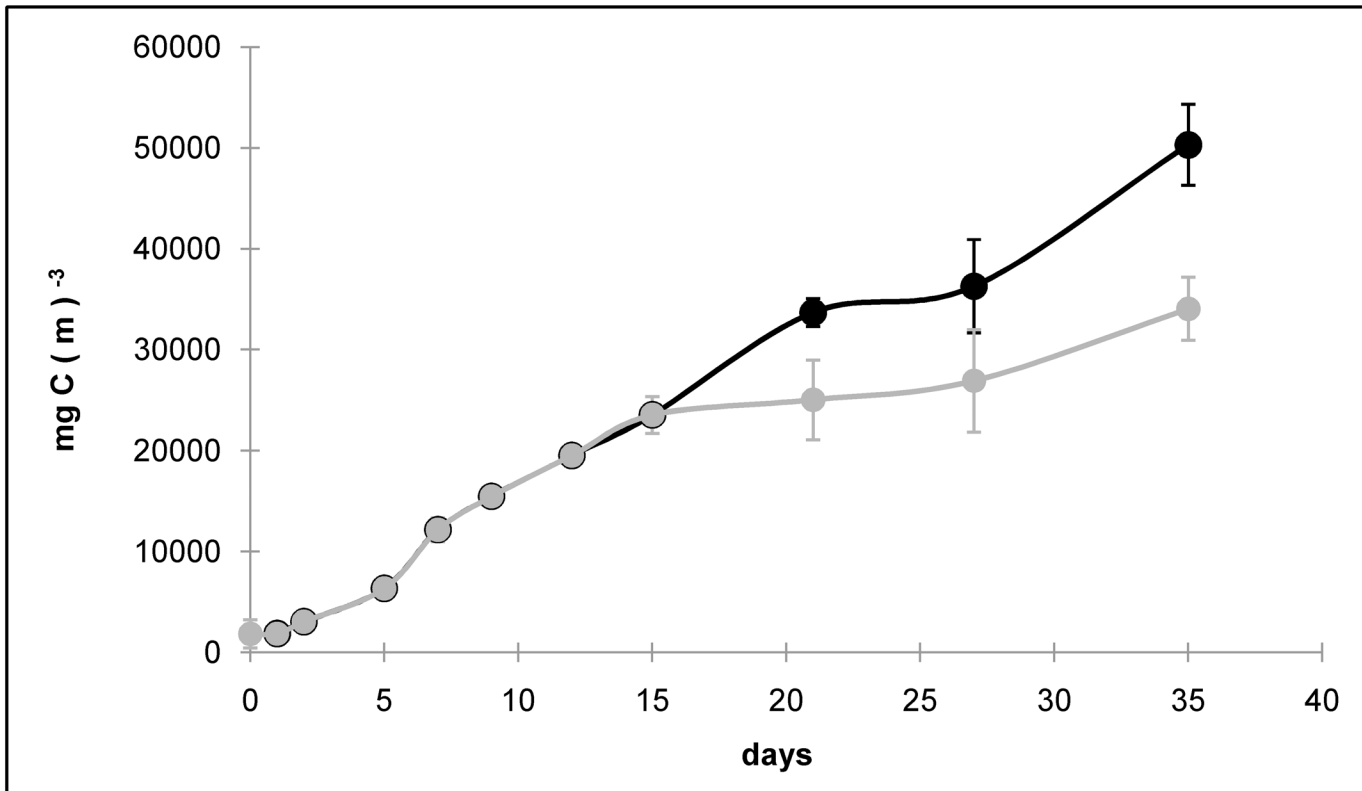


Fig 1. Growth curve of *O. cf. ovata* observed in the cultures. Black spots represent the POC biomass originally detected by CHN analyzer, while the grey ones are the values corrected through regression.

doi:10.1371/journal.pone.0139046.g001

Toxins. Toxins produced in the cultures were treated as a single “generic” toxic compound with elemental formula $C_{129.66} H_{224.32} N_3 O_{52.53}$. This generalization (which was necessary for model comparison, see next section) is plausible considering that the observed toxins (isobaric-palytoxin, ovatoxin-a, -b, -c, -d, -e) were similar in terms of both molecular structure and stoichiometry (129–131 atoms of C, 223–227 atoms of H, 3 atoms of N, 52–54 atoms of O) and that their relative proportions were stable throughout the experiment as previously observed [6,35]. The relationship observed between toxin cellular content (given as toxin to carbon ratio) and cellular nutritional status (given as carbon to nutrients ratios) is displayed in Fig 2.

The model

Model equations (largely derived from Blackford et al. [21]) are given in Appendix A (S1 File). Here we present the equations of toxin dynamics and the ERSEM equations which have been modified with respect to Blackford et al. [21]. Model parameters are listed in Table 1.

Toxin production and fate. Toxic compounds were modelled through two distinct state variables: *tox*, indicating cellular toxins, and *toxe*, indicating extra-cellular toxins. Production of cellular toxin was assumed to be composed of two additive terms. The first term accounts for a constant (moderate) production assumed to be dependent on the newly photosynthesized carbon and takes place under any nutrient conditions. The second term depends on biomass and it is only active under intra-cellular nutrient limiting conditions, represented as internal

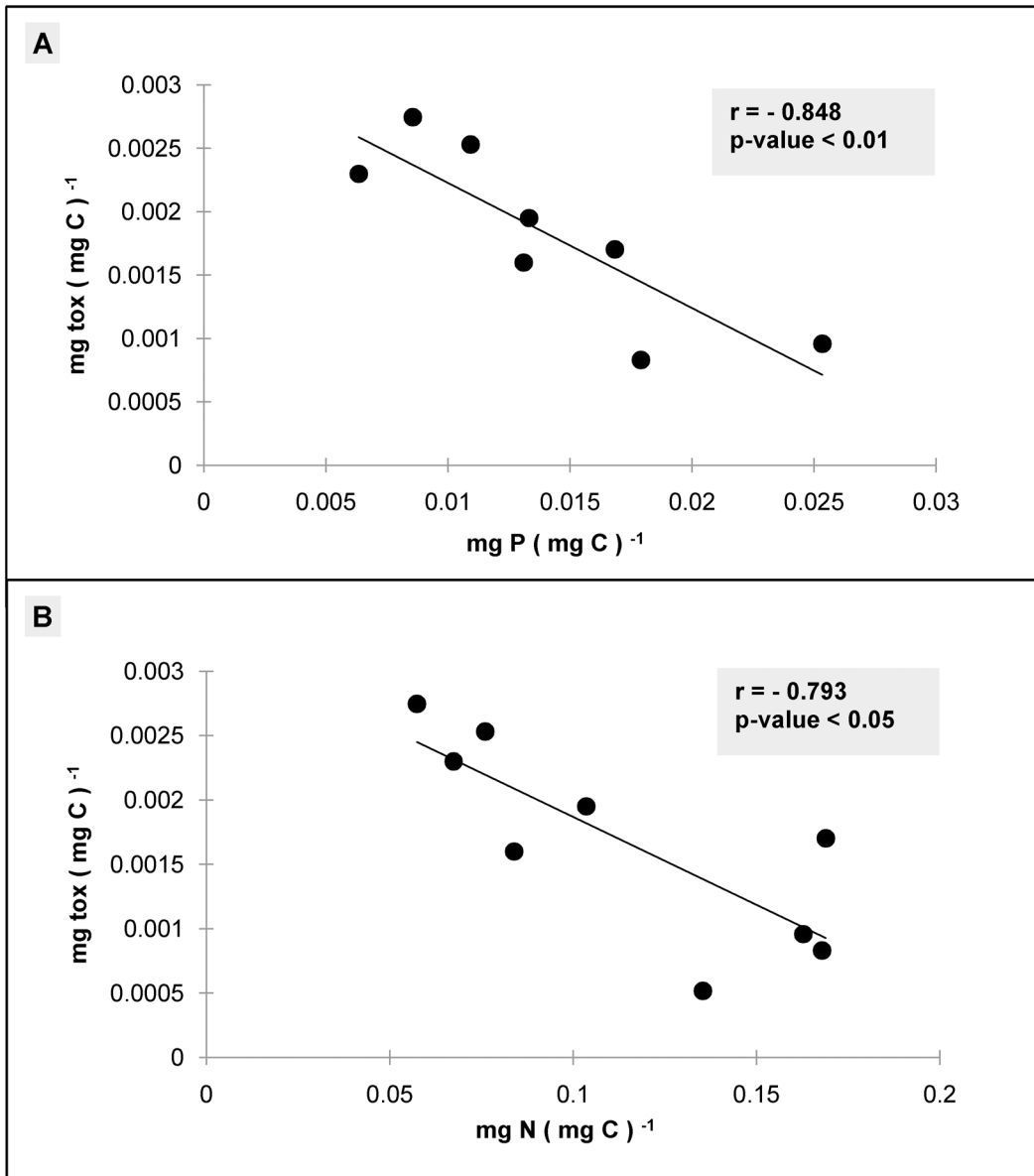


Fig 2. Relationship between toxin to carbon ratio and phosphorus (A) and nitrogen (B) to carbon ratios observed in the experiment presented in Pezzolesi et al. [20].

doi:10.1371/journal.pone.0139046.g002

nutrient to carbon ratio:

$$\left. \frac{\partial \text{tox}}{\partial t} \right|^{INC} = [(GPP - A.RES - EXU) \cdot Q_{Tmin}]_{basal} + \left[(1 - NS) \cdot \left(1 - \frac{Q_T}{Q_{Tmax}} \right) \cdot P^C \cdot \varphi \right]_{stress} \quad (1)$$

where *GPP* is the gross primary production, *A.RES* is the activity respiration and *EXU* is the “physiological” exudation associated with the gross primary production. Q_{Tmin} , Q_T , and Q_{Tmax} are the minimum, actual and maximum toxin to carbon ratio, respectively; P^C is the algal biomass; φ is the fraction of cellular carbon daily invested in the production of *tox* during

Table 1. Model parameters.

Parameter description	Notation	Unit	Value	Reference
Optical and photosynthetic parameters				
Background extinction	σ_{bg}	m^{-1}	0.06	This work
Extinction coefficient of semi-labile DOM	σ_{sl}	$m^2 (mg C)^{-1}$	1 E-5	This work
Extin. coeff. of POM	σ_{POM}	$m^2 (mg C)^{-1}$	1 E-4	[21]
Extin. coeff. of algal biomass	σ_P	$m^2 (mg C)^{-1}$	4 E-4	[21]
Max. spec. photosynthetic rate	r_{ass}	d^{-1}	1.5	[21]
Max. Chl/C cell ratio	θ_{max}	$mg Chl (mg C)^{-1}$	0.02	[37]
Initial slope of PI-curve	α	$mg C m^2 (mg Chl W d)^{-1}$	2.5	This work
Photo-inhibition parameter	β	$mg C m^2 (mg Chl W d)^{-1}$	0.04	This work
Other algal parameters				
Q ₁₀ parameter	Q_{10}	-	2	[21]
Basal respiration rate	$r_{B,res}$	d^{-1}	0.01	This work
Minimum lysis rate	r_{lys}	d^{-1}	0.005	This work
Respired fraction of PP	$r_{A,res}$	-	0.25	[21]
Fraction of excreted carbon	$p_{A,exu}$	-	0.2	This work
Minimum N/C ratio	Q_{Nmin}	$mmol N (mg C)^{-1}$	0.003	This work
Redfield N/C ratio	Q_{NRed}	$mmol N (mg C)^{-1}$	7.862 E-4	[17]
Minimum P/C ratio	Q_{Pmin}	$mmol P (mg C)^{-1}$	1.5 E-4	This work
Redfield P/C ratio	Q_{PRed}	$mmol P (mg C)^{-1}$	1.26 E-2	[17]
Min. N/C ratio for Chl synthesis	Q_{Nmin}^{chl}	$mmol N (mg C)^{-1}$	0.00687	This work
Min. P/C ratio for Chl. Synthesis	Q_{Pmin}^{chl}	$mmol P (mg C)^{-1}$	4.288 E-4	This work
Affinity for NO ₃ ⁻	a_{N3}	$m^3 (mg C)^{-1} d^{-1}$	0.01	This work
Affinity for NH ₄ ⁺	a_{N4}	$m^3 (mg C)^{-1} d^{-1}$	0.01	This work
Affinity for PO ₄ ³⁻	a_P	$m^3 (mg C)^{-1} d^{-1}$	0.01	This work
N-stress threshold	S_N	-	0.6	This work
P-stress threshold	S_P	-	0.6	This work
N-threshold for max. uptake	S_N^{upt}	-	0.95	This work
P-threshold for max. uptake	S_P^{upt}	-	1.2	This work
N-stress threshold for chlorophyll synthesis	S_N^{chl}	-	0.95	This work
P-stress threshold for chlorophyll synthesis	S_P^{chl}	-	1.2	This work
N-stress threshold for respiration decrease	S_N^{res}	-	0.56	This work
P-stress threshold for respiration decrease	S_P^{res}	-	0.51	This work
Carbon fraction invested in basal toxin production	Q_{Tmin}	-	0.001	This work
Maximum tox:C ratio	Q_{Tmax}	-	0.003	This work
Carbon fraction invested in toxin production under nutrient stress	ϕ	d^{-1}	0.0025	This work
Bacterial and organic matter parameters				
Q ₁₀ parameter for bacteria	Q_{10B}	-	2	[21]
Max spec. uptake rate	r_{ass}^B	d^{-1}	4	[21]
Respired fraction of uptake	$r_{A,res}^B$	-	0.6	This work
Respired fraction of uptake under low oxygen	r_{resox}^B	-	0.2	[21]
Basal respiration at 10°C	$r_{B,res}^B$	d^{-1}	0.05	This work
Mortality rate	r_{lys}^B	d^{-1}	0.05	[21]
Half saturation constant for oxygen limitation	h_{ox}	-	0.312	[21]
Maximum N/C ratio	Q_{Nmax}^B	$mmol N (mg C)^{-1}$	0.017	[39]
Maximum P/C ratio	Q_{Pmax}^B	$mmol P (mg C)^{-1}$	0.0018	[39]
Half saturation constant for NH ₄ uptake	h_N	$mmol N m^{-3}$	0.5	[21]

(Continued)

Table 1. (Continued)

Parameter description	Notation	Unit	Value	Reference
Half saturation constant for PO ₄ uptake	h_p	mmol P m ⁻³	0.2	This work
Fraction of labile DOM derived from lysis and exudation	r_{detr}	-	0.25	This work
Breakdown of semi-labile to labile DOM	r_{dis}	d ⁻¹	0.01	This work
Toxin degradation rate	t_{deg}	d ⁻¹	0.1	This work

doi:10.1371/journal.pone.0139046.t001

nutrient-stress conditions. NS is the function describing nutrient limitation and is given by:

$$NS = MIN(NS_p, NS_N) \tag{2}$$

$NS_i (i = N, P)$ is given by:

$$NS_i = MIN \left\{ 1, MAX \left[0, \frac{Q_i - Q_{i\ min}}{(S_i \cdot Q_{i\ Red}) - Q_{i\ min}} \right] \right\} \tag{3}$$

where $Q_i (i = N, P)$ are the actual nutrient to carbon ratios and $Q_{i\ min}$ are the minimum nutrient to carbon ratios, respectively [36]. $S_i (i = N, P)$ are threshold-parameters which determine the nutrient to carbon ratios, given as fraction of the Redfield ratios [18], that enhance the cell production of toxin.

It should be stressed that both tox and $toxe$ are modelled through their carbon content. This implies that toxin nitrogen content is assumed negligible with respect to the total cellular nitrogen budget. Toxin loss terms were assumed to be composed of lysis, basal respiration and nutrient stress-driven exudation:

$$\frac{\partial tox}{\partial t} \Big|^{LOSS} = \left(r_{lys} + \frac{B.RES}{PC} + \frac{S.EXU}{PC} \right) \cdot tox \tag{4}$$

where r_{lys} is the lysis rate, $B.RES$ is the basal respiration (Eq 10) and $S.EXU$ is the nutrient stress-driven exudation [21] (Eq 10a in S1 File).

The amount of toxins released outside the cell is channeled into $toxe$:

$$\frac{\partial toxe}{\partial t} \Big|^{INC} = \left(r_{lys} + \frac{S.EXU}{PC} \right) \cdot tox \tag{5}$$

We assumed that released toxins become part of the dissolved organic pool and are degraded by bacteria with a temporal delay:

$$\frac{\partial toxe}{\partial t} \Big|^{loss} = UPTAKE_B \cdot t_{deg} \cdot \frac{toxe}{DOC} \tag{6}$$

where $UPTAKE_B$ is the bacteria uptake of DOC (see S1 File), t_{deg} is the toxin degradation rate (see Table 1) and DOC is the concentration of the labile dissolved organic carbon.

Chlorophyll, basal respiration and mortality. We modified the chlorophyll dynamics described in Blackford et al. [21] to reproduce better the observed temporal evolution of chlorophyll and the chlorophyll to carbon ratio. The dependence of chlorophyll production on nutrient stress was modelled by introducing a new factor NS^{chl} accounting for nutrient limitation in the source equation of chlorophyll synthesis:

$$\frac{\partial chl}{\partial t} \Big|^{INC} = (PHOTOSYNTHESIS - A.RES) \cdot \rho \cdot NS^{chl} \tag{7}$$

where *PHOTOSYNTHESIS* is the gross primary production (Eq 5a in [S1 File](#)) and *A.RES* is the activity respiration (Eq 12a in [S1 File](#)). ρ is the variable fraction of freshly synthesized carbon invested in chlorophyll synthesis [37] (see Eq 7a in [S1 File](#)). NS^{chl} is given by:

$$NS^{chl} = \text{MIN}(NS_p^{chl}, NS_N^{chl}) \tag{8}$$

NS_i^{chl} ($i = N, P$) is given by:

$$NS_i^{chl} = \text{MIN} \left\{ 1, \text{MAX} \left[0, \frac{Q_i - Q_{i \text{ min}}^{chl}}{(s_i^{chl} \cdot Q_{i \text{ Red}}) - Q_{i \text{ min}}^{chl}} \right] \right\} \tag{9}$$

where $Q_{i \text{ min}}^{chl}$ ($i = N, P$) are the minimum nutrient to carbon ratios for chlorophyll synthesis and s_i^{chl} are factors that determine the fraction values of the Redfield nutrient to carbon ratios at which the chlorophyll synthesis starts to decrease.

We re-formulated the ERSEM equations describing lysis and basal respiration in order to reproduce the biomass concentration observed in the last part of the experiment. In comparison to Blackford et al. [21] the lysis rate was reduced (see [Table 1](#)) and assumed to be independent of nutrient stress (Eq 8a in [S1 File](#)). This choice was driven by the observation of a very small number of dead cells in the cultures, which suggested that *O. cf. ovata* was only marginally affected by lysis in the investigated system.

A reduction of basal respiration under extreme nutrient limiting conditions was assumed, to mimic the formation of resting stages [38]:

$$B.RES = f^T \cdot r_{B.res} \cdot NS^{res} \cdot P^C \tag{10}$$

where f^T is the function describing the metabolic dependency from temperature [21] (Eq 3a in [S1 File](#)) and $r_{B.res}$ is the basal respiration rate. The value of the limiting factor NS^{res} varies between 0.1 and 1, and is given by:

$$NS^{res} = \text{MIN} \{ 1, \text{MAX} [0.1, \text{MIN} (NS_p^{res}, NS_N^{res})] \} \tag{11}$$

where NS_i^{res} ($i = N, P$) is given by:

$$NS_i^{res} = \frac{Q_i - Q_{i \text{ min}}}{(s_i^{res} \cdot Q_{i \text{ Red}}) - Q_{i \text{ min}}} \tag{12}$$

where s_i^{res} are multiplying factors which describe the fraction values of the Redfield nutrient to carbon ratios at which the basal respiration rate starts to decrease.

Finally, given the high concentration of dissolved polysaccharides observed in the cultures, we assumed that the semi-labile dissolved organic carbon (R_{sl}^C) excreted by the alga was able to reduce the available light, following the equation describing light extinction reported in Appendix A (Eq 1a in [S1 File](#)).

Sensitivity analysis with respect to selected processes

A process-based sensitivity analysis was performed by modifying the formulation described above and assessing the consequent changes in model outputs. More specifically, three simulations S1-S3 were carried out by “switching off” three key processes directly linked to our model assumptions: S1) the reduction of basal respiration under extreme nutrient limiting conditions (Eq 10); S2) the nutrient stress-induced reduction of chlorophyll synthesis (Eqs 7 and 8) and S3) the enhanced production of toxin triggered by nutrient stress (Eq 1). An additional simulation was carried out by removing the bacteria component from the model. Results were compared with the reference simulation and with the experimental data in order to quantify to

what extent the above mentioned processes and the presence of bacteria affected the simulation of *O. cf. ovata* growth and in particular toxin dynamics.

Sensitivity analysis with respect to model parameters

A quantitative sensitivity analysis was carried out to rank the importance of the model parameters in determining the model output. We applied a Monte-Carlo based approach (e.g. [40,41]) to rank the sensitivity of the simulated maximum value of the concentration of intracellular toxin with respect to the model parameters listed in Table 1. The m model parameters X_j are collected in the “input factor” vector, $\mathbf{X}_i = (X_1, \dots, X_j, \dots, X_m)$, $i = 1, 2, \dots, n$. A number $n = 1000$ random realizations of the vector was obtained by sampling uniform probability distributions defined for each of the parameters. The range of such distributions was set equal to $\pm 30\%$ of the reference values of the parameters listed in Table 1. The 30% variation with respect to the reference values of the parameters is often assumed in sensitivity analyses of environmental models when the real ranges are unknown (see, e.g., Ciavatta et al. [42]). We considered the 30% range to be reasonable also for the parameters of our model. Each random realization was used to run a model simulation that provided a scalar output y_i . The parameter-to-output relationship was represented by means of a multiple linear regression model $\mathbf{y} = \mathbf{X} \mathbf{b} + \boldsymbol{\varepsilon}$. The absolute values of the standardized regression coefficients, $|\beta_j|$, are the sensitivity indexes that provide the rank of the input factors (e.g., [41,43]). We note that the regression coefficients provide meaningful rankings of the parameters only when the linear regression explains a relatively large fraction of the variability of the model output [43]. We assessed the applicability of the linear regression by computing the fraction of explained variance (R^2), the regression significance (F-statistic of the null hypothesis of constant model, $p < 0.01$), as well as the significance of the standardized regression coefficients (t-statistic, $p < 0.05$).

Comparison with literature data

Literature on C-rich toxin producers was reviewed and datasets suitable for model validation were selected. The observational values used for model comparison were obtained by using data describing the carbon to phosphorous ratios (C:P) and the carbon associated with toxin as a percentage of total carbon (C-tox:C) $\times 100$ observed in different strains of *Karenia brevis* [44,45]. Data related to N-limitation were taken from table 2 (C:N) and from Figs 1F and 2F [(C-tox:C) $\times 100$] of Hardison et al. [44]. Data related to P-limitation were taken from Table 3 of Hardison et al. [45]. The increase of cellular toxin for each strain considered was obtained by dividing the values of (C-tox:C) $\times 100$ observed under nutrient depletion conditions by the same values observed under nutrient replete conditions. The increments of toxin were then averaged (and the standard deviation was computed) over all the strains investigated. Overall, we used 10 values of C:P and (C-tox:C) $\times 100$ (each of them given as average of three replicates, [45]) to assess the model performance under P-limitation and 4 values of C:N and (C-tox:C) $\times 100$ (each of them given as average of three replicates, Hardison et al. [44]) to assess the model performance under N-limitation. For this comparison, the model was run with the initial phosphate and nitrate concentrations reported in Hardison et al. [44,45] and without bacteria component. We also assumed balanced initial conditions for chlorophyll and internal toxin. The simulated toxin to carbon ratios were normalized by the value assumed to represent the toxin to carbon ratio under balanced growth (0.001, see Table 1 and Eq 1).

Results

Model simulations and comparison with experimental data

The comparison between model simulation and experimental data is shown in [Fig 3](#). All the model outputs were in good agreement with the experimental data, as highlighted by the high values of the correlation coefficient reported in the figure.

The simulated evolution of the algal biomass ([Fig 3A](#)) depicted a “classic” growth curve. After a first phase of acclimation (days 0–3), biomass started to increase exponentially (days 3–9) reaching a stable value ($\sim 25 \text{ g C m}^{-3}$) after 15 days (stationary phase). The model simulation reproduced the observed pattern well, with the exception of the last value (day 35), which was underestimated by the model. Simulated chlorophyll concentration (panel B) peaked on day 8, reaching 185 mg m^{-3} . Afterwards, chlorophyll decreased monotonically down to 42 mg m^{-3} at day 35. The model reproduced well the observed pattern of chlorophyll until day 21. However, the observed chlorophyll increased again in the last two sampling days (27 and 35), reaching a value of $\sim 100 \text{ mg m}^{-3}$ at the end of the experiment. Simulated chlorophyll to carbon ratio (Chl:C, panel C) displayed a behavior similar to the modelled chlorophyll and is in good agreement with the observations. Carbon to nutrient ratios (panels D and E) simulated by the model presented a sharp increase from day 5 (phosphorus) and 9 (nitrogen). The carbon to nitrogen ratio stabilized after day 21 (reaching a value of 12 mol mol^{-1}) while the carbon to phosphorus ratio increased until the end of the experiment (when it reached a value of $\sim 270 \text{ mol mol}^{-1}$). Model simulations reproduced well the observed dynamics although underestimating the carbon to nitrogen ratio in the second half of the experiment.

External toxin concentration (panel F) was detectable only after 9 days and reached its maximum value ($\sim 15 \text{ mg m}^{-3}$) at day 27 while it decreased to 6 mg C m^{-3} at the end of the experiment. Model simulation was in qualitatively good agreement in terms of both magnitude and qualitative behavior until day 28, but it overestimated the observed values in the last part of the experiment (15 mg m^{-3} simulated against 8 mg m^{-3} observed). The correlation between observed and simulated external toxin was the only one that was not significant ($p = 0.07$), probably as a consequence of the relatively small number (6) of available data points.

Cellular toxin and toxin to carbon ratio are displayed in panels G and H, respectively. The toxin concentration (spanning from 1 to 70 mg C m^{-3}) seemed to follow the temporal evolution of carbon (panel A) and is in good agreement with the observations. The simulated toxin to carbon ratio increased steadily until day 27, consistently with the observed values. The increase of the toxin to carbon ratio was slow in the first days of the culture and it became steeper after day 10, concomitantly with the observed decrease in chlorophyll and chlorophyll to carbon ratio and the increase in carbon to nutrient ratios. The model simulated a toxin to carbon ratio ranging from 0.5 to 1 ($\mu\text{g C mg C}^{-1}$) in correspondence of C:P and C:N ratios ranging from 100 to 150 and 8 to 6 (mol mol^{-1}), respectively. Simulated toxin to carbon ratio increased up to 2.8 ($\mu\text{g C mg C}^{-1}$) concomitantly with a C:P and C:N ratios ranging from 180 to 270 and 7 to 12 respectively. Simulated bacteria ([Fig 4](#)) were very close to the observations in the first 15 days of the culture. From day 15 to day 30 the model simulated a maximum of biomass ($\sim 1350 \text{ mg C m}^{-3}$ at day 28) and then a (slowly) declining phase. To the contrary, observed bacteria were monotonically increasing even at the end of the culture.

Sensitivity analysis with respect to processes

The results of the sensitivity simulations S1, S2 and S3 ([Fig 5](#)) showed that all the investigated processes significantly improved the simulations, taking the model output closer to the observed values. As expected, the reduction in basal respiration (S1) affected only the

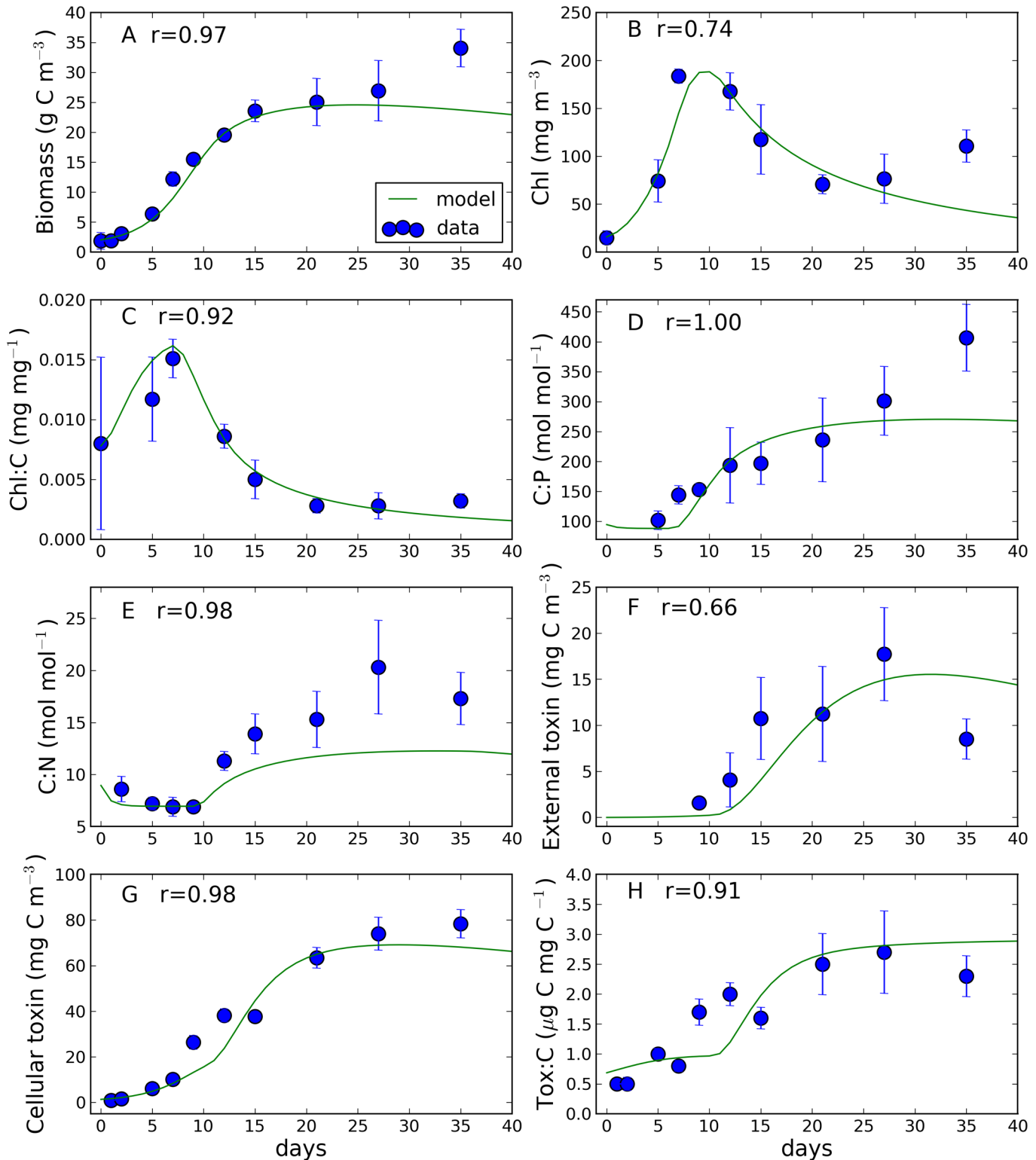


Fig 3. Comparison between observed and simulated (A) algal biomass (Biomass), (B) chlorophyll (Chl), (C) chlorophyll to carbon ratio (Chl:C), (D) carbon to phosphorus ratio (C:P), (E) carbon to nitrogen ratio (C:N), (F) external toxin, (G) cellular toxin and (H) toxin to carbon ratio (Tox:C). Bars indicate standard deviations. In each panel the Spearman rank correlation coefficient (r) between observations and simulations is also displayed. All the correlations are significant ($p < 0.05$) except for panel F.

doi:10.1371/journal.pone.0139046.g003

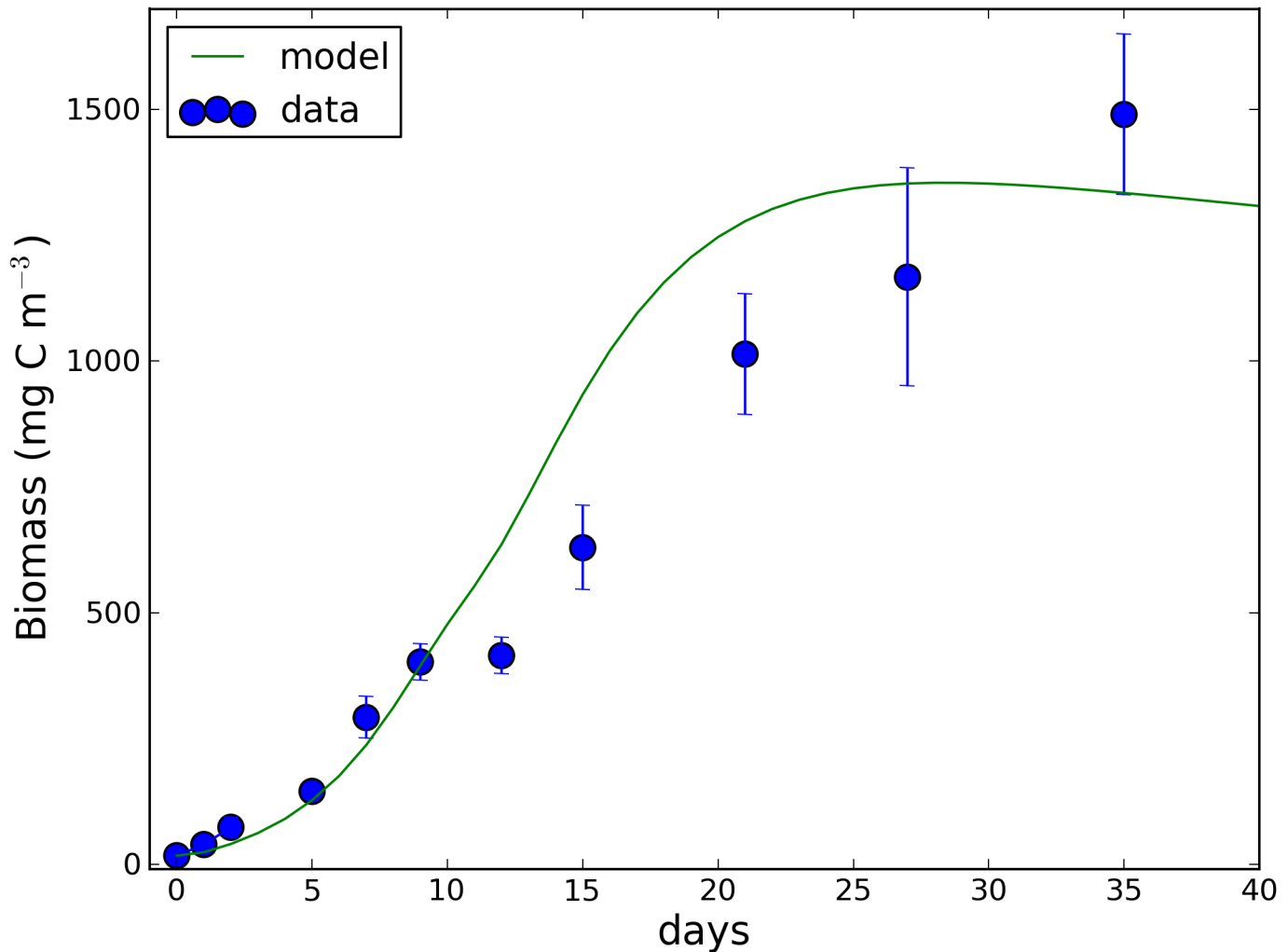


Fig 4. Observed and simulated bacteria biomass.

doi:10.1371/journal.pone.0139046.g004

simulation of the last few days of the experiment, when the nutrient stress was high. Conversely, the nutrient dependent reduction in chlorophyll synthesis (S2) and the nutrient-dependent enhancement of toxin production (S3) affected the simulation since the very beginning of the experiment. The effect of nutrients on chlorophyll synthesis, which was assumed to begin at a relatively high nutrient to carbon internal ratio (see [Table 1](#) and [Fig 6](#)), was also particularly important for the realistic simulation of the chlorophyll to carbon ratio, as evident in [Fig 5B](#). The simulation without bacteria component produced identical results with respect to the simulation with bacteria with the only exception of the external toxin ([Fig 5C](#)). Without bacteria, the model predicted an accumulation of external toxin (reaching 40 mg C m⁻³ at day 35) which was not observed in the experimental data.

Sensitivity analysis with respect to parameters

The Monte-Carlo based sensitivity analysis demonstrated that the parameter describing the maximum toxin threshold (Q_{Tmax}) was the most important in the simulation of our target model variable, i.e. the maximum value of the internal toxin concentrations (see [Table 2](#)). This

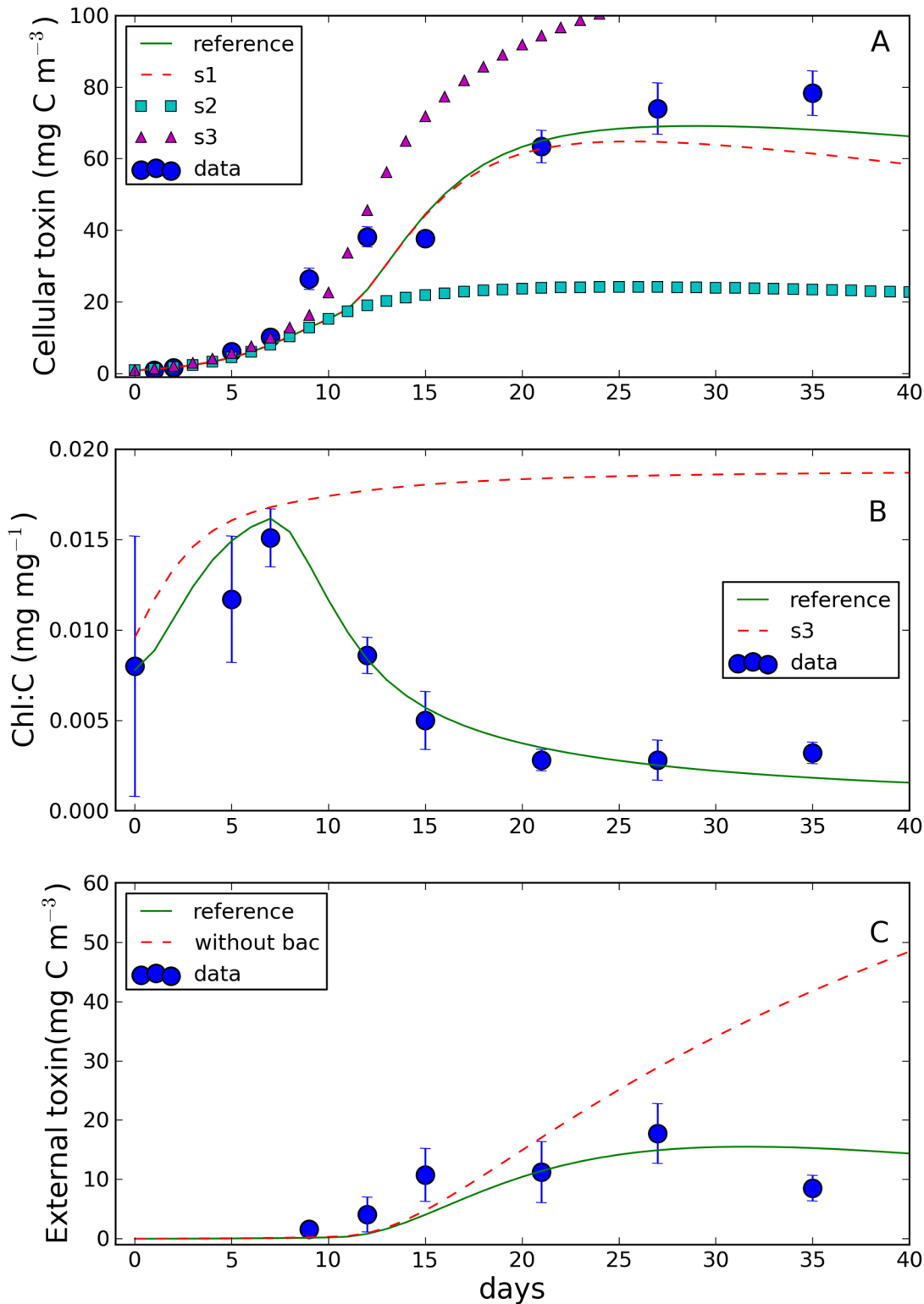


Fig 5. Sensitivity analysis with respect to selected model processes (experiment S1-3, see the text for explanation). (A) simulated and observed intracellular toxin; (B) modelled and observed chlorophyll to carbon ratio (Chl:C). (C) external toxin concentrations simulated with and without bacteria (bac). Data (with standard deviation) are also displayed.

doi:10.1371/journal.pone.0139046.g005

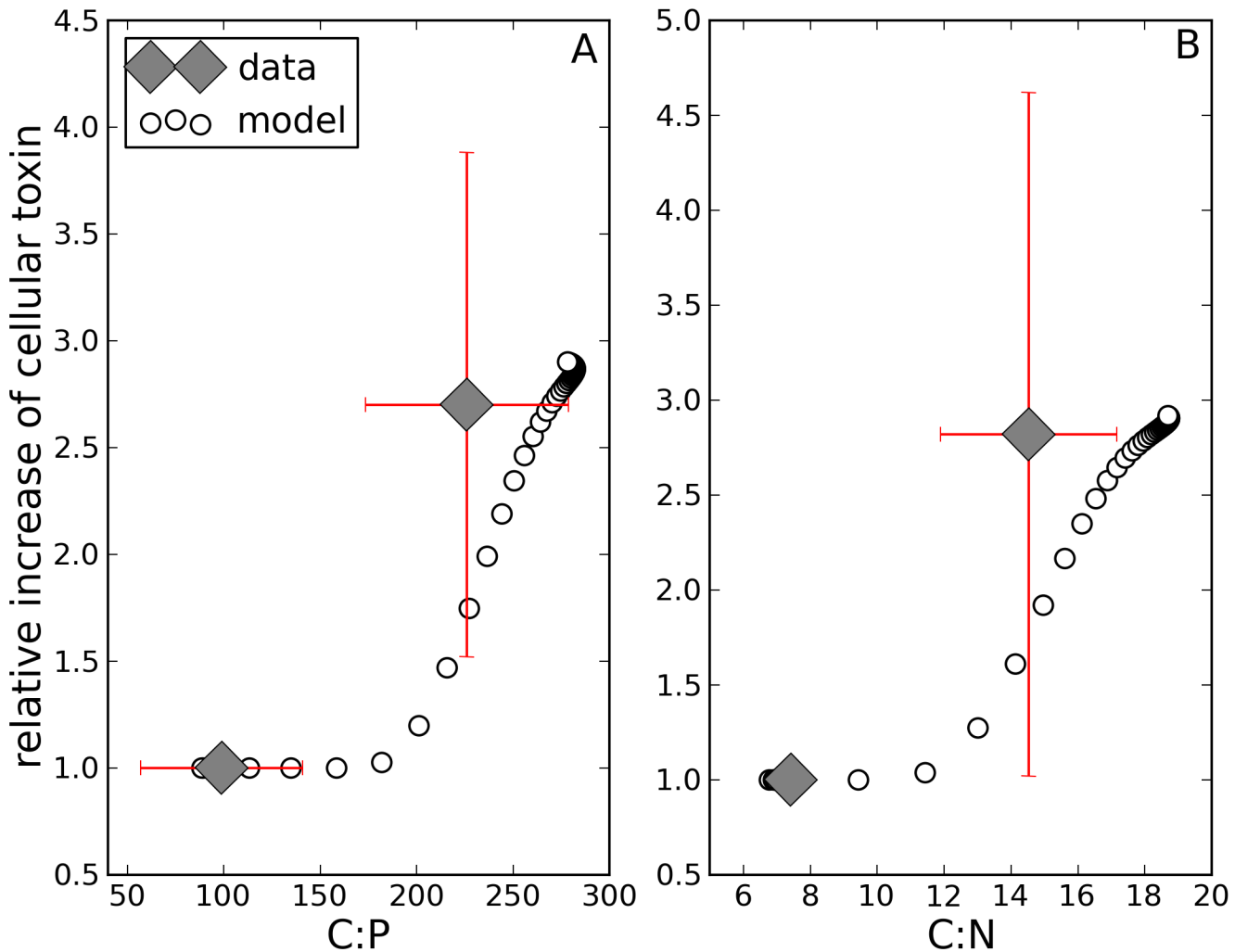


Fig 6. Simulated and observed changes in toxin content in response to C:P (A) and C:N (B) cellular ratios. Simulated toxin to carbon ratios have been normalized by the value of 0.001 (see Table 1 and Eq 1). Diamonds refer to the mean increase in cellular toxin observed in *Karenia brevis* grown under P-limited ([45], panel A) and N-limited ([44], panel B) conditions. The error bars represent the standard deviations.

doi:10.1371/journal.pone.0139046.g006

parameter scored the highest value of the standardized coefficient in the regression analysis of the Monte Carlo simulations. Model parameters describing algal physiology (e.g. S_p , α , $Q_{p\ min}$) and the parameter regulating the amount of semi-labile (light-absorbing) organic carbon in the medium (r_{detr}) were important in simulating the toxin evolution and statistically significant ($p < 0.05$). Model parameters included in the analysis (see Table 1) but not listed in Table 2 did not influence noticeably the toxin concentration, since their regression coefficients were close to zero and were not statistically significant. Importantly, the ranking provided by the sensitivity analysis was trustworthy, since the linear regression explained most of the model output variability ($R^2 = 0.91$), and it was highly significant (F-statistic = 224, $p < 0.01$).

Comparison with literature data

The simulated relative increase of the toxin to carbon ratio (tox:C) as function of internal C:P and C:N ratios is displayed in Fig 6 along with values related to the dinoflagellate *Karenia brevis* estimated from Hardison et al. [44,45]. Model tox:C remained constant until the carbon to

Table 2. Rank of the importance of the model parameters for the target output, i.e. the maximum internal toxin concentration. The rank is based on the absolute values of the standardized regression coefficients ($|\beta|$). The list includes a subset of the model parameters in Table 1, i.e. those that have statistically significant regression coefficients (t-statistic, $p < 0.05$).

	Parameter	Rank	$ \beta $
Q_{Tmax}	Maximum tox:C ratio	1	0.765
S_P	P-stress threshold	2	0.324
r_{detr}	Fraction of labile DOM derived from lysis and exudation	3	0.313
α	Initial slope of PI-curve	4	0.206
Q_{Pmin}	Minimum P/C ratio	5	0.187
$r_{A,res}$	Respired fraction of PP	6	0.111
S_P^{res}	P-stress threshold for respiration decrease	7	0.097
$r_{B,res}$	Basal respiration rate	8	0.088
Q_{10}	Q_{10} parameter	9	0.073
$\rho_{A,exu}$	Fraction of excreted carbon	10	0.069
r_{lys}	Minimum lysis rate	11	0.063
φ	Carbon fraction invested in toxin production under nutrient stress	12	0.055
$Q_N^{chl\ min}$	Minimum N/C ratio for chlorophyll synthesis	13	0.049
S_N^{upt}	N-threshold for max. uptake	14	0.033
S_N	N-stress threshold	15	0.032
σ_P	Extinction coefficient of algal biomass	16	0.0284
Q_{Tmin}	Carbon fraction invested in basal toxin production	17	0.0283
S_N^{chl}	N-stress threshold for chlorophyll synthesis	18	0.023

doi:10.1371/journal.pone.0139046.t002

nutrient ratio reached a value of 170 and 12 (C:P and C:N, respectively). When these threshold values were reached, tox:C increased up to three times with respect to the values simulated under lower C:P and C:N ratios. The relative increase of tox:C observed in *K. brevis* grown under nutrient depletion conditions reached an average value of 2.6 under P-limitation and 2.8 under N-limitation. However, the variability among the different strains considered was remarkable, as indicated by the standard deviation bars shown in Fig 6. The model predicted an increase in tox:C (starting when C:P > ~170) which was consistent with the increase in tox:C observed in *K. brevis* under P-limitation. The agreement between simulated and observed tox:C increase for N-limited condition was less satisfactory since the model predicted a slower increase of tox:C with respect to C:N. The model also simulated C:N values higher than the observed one. It should be stressed, however, that the comparison under N-limitation condition is biased by the reduced number of data used (only two experiments were available).

Discussion

Our modelling analysis provided a conceptual framework describing the feedbacks between nutrient availability and cellular physiology of dinoflagellates species producing C-rich toxins (Fig 7). Notably, our approach described the nutritional cellular stress of the algae by using internal nutrient quota (i.e. carbon to nutrient ratio) rather than the nutrient ratio in the medium and this allowed us to represent cellular stress in a more realistic way [46].

Modelling *O. cf. ovata* physiology

Our model was constructed by analyzing the behavior of the dinoflagellate *O. cf. ovata*, a species representing a new and less known issue compared with other toxic microalgae. The toxins

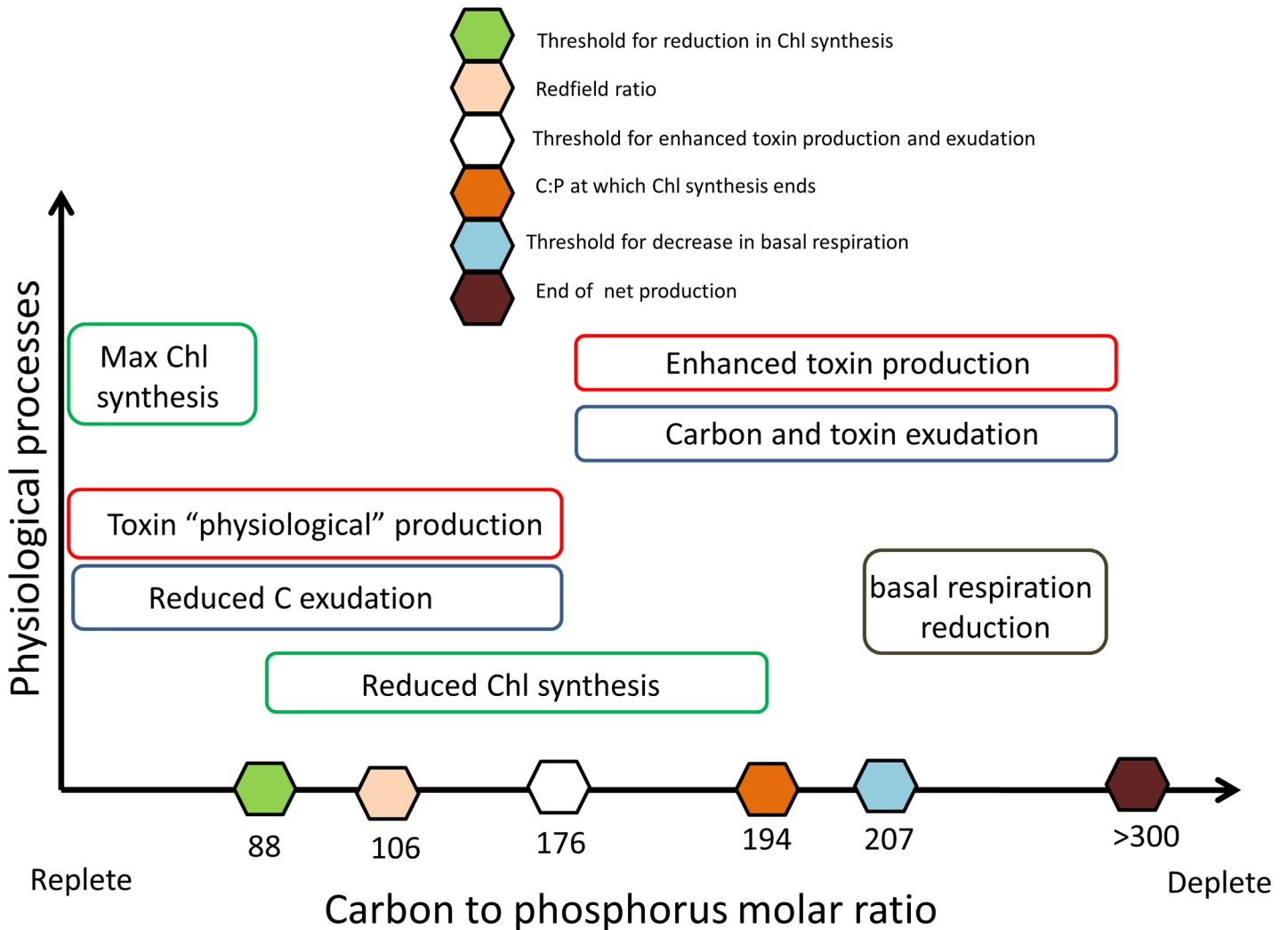


Fig 7. Conceptual model linking algal nutritional status (x-axis) to key physiological processes (y-axis). The sequence of processes triggered by increasing values of the carbon to phosphorus molar ratio, i.e. by shifting from high to low nutrient regimes, can be followed from the left to the right in the scheme. This is also the direction of the temporal evolution of the culture experiment, where nutrients were progressively depleted by the algae.

doi:10.1371/journal.pone.0139046.g007

produced by this organism are characterized by a very high molecular weight, high C:N ratio (about 43), and their production is likely to represent a high cost in carbon and energy terms. Data were obtained from *O. cf. ovata* cultures performed in standard nutrient conditions and followed to a very late stationary phase. This allowed us to investigate the evolution from a nutrient replete to a nutrient limitation state.

Under high nutrient regimes (as simulated in the first few days of culture) *O. cf. ovata* was able to actively grow, synthesizing the different cellular constituents including toxins. During the first 7 days of culture, the algae reached the maximum chlorophyll cellular content and the “physiological” level of toxins. Both chlorophyll and toxin to carbon ratios would stay approximately constant if the condition of light and nutrients were constant (balanced growth). This has already been observed for chlorophyll in cells growing under constant nutrient and light conditions [37,47]. Polysaccharide excretion was kept at a minimum physiological rate (here assumed to be 20% of the gross carbon fixation), and the toxins were not released into the

environment. Under these conditions, we hypothesized that *O. cf. ovata* was performing a phototrophic metabolism while the cellular toxin may act as carbon (and nitrogen) storage.

As soon as the internal nutrient concentration started to decrease (day 7, Fig 3D and 3E), a sequence of physiological adjustments took place. Interestingly, chlorophyll synthesis was the first process undergoing a strong reduction. The model suggested that the carbon invested in photosynthetic compounds started to decrease when the internal nutrient level was higher than the Redfield ratio (Figs 3 and 5). However, when both chlorophyll and chlorophyll to carbon ratio started to dramatically decrease (from day 7, Fig 3), the biomass was still exponentially growing, suggesting that *O. cf. ovata* was able to maximize photosynthetic efficiency even with a reduced light harvesting apparatus.

The reduction in chlorophyll content per cell represents a common response of photosynthetic cells to nitrogen limitation; however, when microalgae are grown under replete conditions, chlorophyll content patterns vary from being stable for days after external nutrients were depleted [48] to decreasing concurrently with external and internal nutrient decrease [49,50]. As reported in other dinoflagellates, the observed chlorophyll to carbon ratio values in *O. cf. ovata* decreased as soon as the C:N ratio started to increase and reached values which are among the lowest reported [51]. This result could be due to a mixotrophic metabolism which allows changes in trophic behavior (in this case driven by cell nutrient state) shifting from a prevailing phototrophic to a prevailing heterotrophic mode for nutrient supplies. Indeed under inorganic nutrient deficiency mixotrophs would strategically survive and grow getting organic N and P by osmotrophy and/or phagotrophy [52,53] and thus, from this perspective, chlorophyll biosynthesis could become a negative energetic cost-benefit investment as suggested by Raven [54].

In the investigated system, the contribution of the dissolved organic matter to *O. cf. ovata* nutrition could not be assessed. However, the ability of this species to utilize organic matter is testified by the enhancement of alkaline phosphatase activity under P-limitation recently reported [55]. Moreover, the absence of prey items of a suitable size range in the system did not allow us to test the contribution of nutrients' supply from phagotrophy. Indeed, while micro-predation has been proposed for this alga [56] and observed for other *Ostreopsis* species preying on naked ciliates [57], predation on bacterial cells would require feeding strategies [53] not yet assessed for *Ostreopsidaceae* species.

Bacteria could also impact algal dynamics by making nutrients available to the algae, according to their more traditional role as remineralizers or by competing for nutrients. However, the model simulation run without the bacteria component did not change the results shown in Fig 3, with the exception of the external toxin concentration (Fig 5C), as previously hypothesized by Vanucci et al. [58]. This suggests that bacteria, while actively assimilating the toxin in the medium are not significantly impacting on algal growth and toxin production. However, given the complexity of the algal-bacteria interactions which go well beyond the competition for nutrients [59,60], additional experiments are required to better conceptualize and model the role played by bacteria on the growth and toxicity of *O. cf. ovata*.

With the progression of *O. cf. ovata* growth, the level of cellular nutrients further decreased, from day 10–11 onwards (C:P ratio >175), and the investment in toxins was enhanced concomitantly with an enhanced release of both carbon and toxins into the environment. It is interesting to note that the increased production of toxins and their external release began at a lower nutrient level with respect to the decrease in chlorophyll synthesis, suggesting that *O. cf. ovata* was entering into a “phase two” of its strategy to face adverse nutrient conditions. The cells increased the toxin content until approaching a critical toxin to carbon ratio represented by the parameter Q_{Tmax} . Importantly, the model assumed that the enhanced production of toxins depended on the biomass standing stock and not on its production rate. This suggests that

this alga is able to synthesize toxins from carbon previously photosynthesized and to produce toxins even when the environmental conditions do not allow a net growth. The observed behavior is in agreement both with the carbon to nutrient balance hypothesis (and thus with the idea that carbon surplus in plant cells is utilized to build up defense mechanisms), and with the reported observation that C-rich toxins generally increase under N and P limitation [4].

The relative importance of nitrogen or phosphorus in this species was difficult to assess because the two nutrients were depleted nearly at the same time so that in our experimental system we observed a toxin increase when both C:P and C:N were higher than the Redfield ratio.

The increase in intracellular toxin could represent a mechanism to discourage predation, as already proposed [46,61,62]. In this way, *O. cf. ovata* could limit top down control when the environment is strongly limiting because of the low level of nutrients, i.e. when it is bottom up controlled. This strategy could allow the algae to keep a sizable background concentration from which it is possible to re-build a healthy population when the environmental conditions revert back to positive. The extrusion of polysaccharide matrices and toxins along with the decrease in cellular nutrient content (accumulation of carbon) are all factors potentially acting as deterrents for grazers [5,20,25,63,64].

When the cellular nutrient to carbon ratio further decreased (C:P >207 in Fig 5), a third process entered into play. In the last days of the culture, C:P and C:N intracellular molar ratios reached extreme values, being very far from the values of 106 and 6.6 proposed by Redfield [17,18] as mean values for marine microalgae. In order to reproduce such low nutrient values we had to assume reduced metabolic losses (basal respiration and mortality rates). In particular, a progressive (reversible) reduction in basal respiration rate, starting from a carbon to phosphorus ratio of ~200 was necessary for the model to simulate the high concentration of algal biomass and toxins observed at the end of the culture (Fig 4). The need to include this process supports the hypothesis that *O. cf. ovata* forms resting stages at extremely limiting nutrient conditions [65,66].

The sensitivity analysis (Table 2) identified the most important parameters for the simulation of the maximum value of toxin. The analysis highlighted that the parameter regulating the maximum amount of cellular toxin (Q_{Tmax}) should be estimated with great care to adequately simulate the intracellular toxin concentration. Notably, the analysis revealed that the parameters regulating the physiology of the alga (e.g. photosynthetic parameters, parameters regulating internal nutrient level, loss terms etc.) are also very important. This information is valuable to properly calibrate the model when, in future works, we will apply it in realistic marine ecosystem simulations. Finally, we noted that most of the new parameters introduced into the model ranked relatively low in the sensitivity analysis. This suggests that the good agreement between data and simulations was not due to an over-parameterization of the model, but to the inclusion of key processes in the model structure.

Model validation and applicability

In order to assess to what extent the proposed model could be applicable to other species producing C-rich toxin, we have compared model simulations with the data reported in the literature for *Karenia brevis*, a dinoflagellate producing brevetoxin (classified as C-rich toxin [4]). Although the absolute value of the C-toxin as a percentage of the total carbon was much higher in *K. brevis* (up to 5%) than in *O. cf. ovata* (<1%), the trend and the value of the relative increase of the tox:C ratio as function of carbon to nutrient ratios simulated by the model was in good agreement with the observations (Fig 6). We have used the dataset reported in Hardison et al. [44,45] as it was among the few including measurements of toxin to carbon ratios and carbon to nutrient ratios which are required for a quantitative model comparison. However,

from a more qualitative point of view, our model is in agreement with other observations regarding C-rich toxin producing dinoflagellates. For example, Adolf et al. [67], studying toxin production in 6 different strains of *Karlodinium veneficum* (producing the C-rich karlotoxin), observed high values of cellular toxin concentration (up to 21 pg of toxin per cell) under high C:P values (up to 470). These values when normalized by the values corresponding to more balanced C:P (i.e. C:P closer to the Redfield ratio) gave a relative increase ranging from 2.7 to 10.7. Johansson et al. [68] observed an increase in okadaic acid production in *Dynophysis acuminata* when cultured under N and P-limiting conditions. More specifically the mass of okadaic acid per cell with respect to the nutrient replete culture increased by a factor 4.3 and 20 for P-limited and N-limited conditions, respectively. Johansson and Granéli [69], when studying *Chroschro-mulina polylepis*, observed an increase of a factor 2 in the algal toxicity (given as hemolytic activity), concomitantly with a variation of the C:P ratio from 111 to 249.

The absolute values of internal toxins (and the associated toxicity) are regulated in the model by the parameters Q_{Tmax} and Q_{Tmin} . These parameters are highly variable among microalgae and even within different strains of the same species [44,45,70,71,72]. For this reason, in order to assess the model capacity to simulate a general behavior, we have normalized the toxin quota observed (and modelled) under high carbon to nutrient ratio by the values observed (and modelled) under balanced growth. Results shown in Fig 6 and the broad comparison with the literature highlighted that the model is able to reproduce a behavior widely observed among toxic dinoflagellates. This means that the model can be used to simulate the stoichiometric regulation of C-rich toxins in different dinoflagellates when species-specific parameters (i.e. Q_{Tmin} and Q_{Tmax}) are properly tuned.

Finally, we recall that our model only describes the relationship between nutrients (throughout the cellular nutritional status) and toxin production, and it does not account for other biotic processes, such as grazing, which can also stimulate toxin production in dinoflagellates [73,74]. These factors are important to fully understand the environmental regulation of toxin production and should be considered in future model developments meant to simulate algal toxicity in a realistic ecosystem framework.

Conclusions

We have developed a numerical model by interpreting experimental data describing growth and toxin production in *O. cf. ovata*. By analyzing model simulations and comparing them with experimental data, we have provided a conceptual framework linking the nutritional status to toxin production in this alga. In particular, we have identified four physiological processes directly associated with an increasing state of intra-cellular nutrient stress (increase of C:P and C:N cellular ratio): i) a sharp decrease in chlorophyll synthesis ii) an enhancement of toxin production, iii) the release (exudation) of toxin in the environment and iv) a reduction in metabolic maintenance leading to the formation of resting stages.

By comparing model simulations with literature data, we have highlighted that our model has the potential to simulate the stoichiometric regulation of C-rich toxins in different marine dinoflagellates. The next step will be to implement the presented formulation in a comprehensive ecosystem modeling framework (for example the ERSEM-GOTM system [21]) and to use it to investigate and predict the effect of nutrient supply in the formation and evolution of harmful algal blooms.

Supporting Information

S1 Fig. Relationship between cell carbon and cell volume.
(TIF)

S1 File. Appendix A (Model equations).
(DOCX)

S2 File. Dataset (Experimental data).
(XLSX)

S3 File. Dataset (Model simulations).
(XLSX)

S4 File. Dataset (Model simulations).
(XLSX)

S5 File. Dataset (Model simulations).
(XLSX)

Acknowledgments

We would like to thank Dr Susan Key for help proofreading the manuscript.

Author Contributions

Conceived and designed the experiments: L. Polimene RP. Performed the experiments: AP L. Pezzolesi SV. Analyzed the data: L. Pezzolesi AP SV. Wrote the paper: L. Polimene L. Pezzolesi AP SC SV RP. Sensitivity analysis: SC.

References

1. Anderson DA, Cembella AD, Hallegraeff GM. Progress in understanding harmful algal blooms: paradigm shifts and new technologies for research, monitoring, and management. *Annu Rev Mar Sci.* 2012; 4: 143–176.
2. Davidson K, Gowen RJ, Harrison PJ, Fleming LE, Hoagland P, Moschonas P. Anthropogenic nutrients and harmful algae in coastal waters. *J Environ Manage.* 2014; 146: 206–216. doi: [10.1016/j.jenvman.2014.07.002](https://doi.org/10.1016/j.jenvman.2014.07.002) PMID: [25173729](https://pubmed.ncbi.nlm.nih.gov/25173729/)
3. Pistocchi R. Factors affecting algal toxicity. In: Rossini GP, editor. *Toxins and biologically active compound from microalgae.* CRC Press, Taylor & Francis Group, London; 2014. pp. 75–96.
4. Van de Waal DB, Smith VH, Declerck SAJ, Stam ECM, Elser JJ. Stoichiometric regulation of phytoplankton toxins. *Ecol Lett.* 2014; 17: 736–742. doi: [10.1111/ele.12280](https://doi.org/10.1111/ele.12280) PMID: [24712512](https://pubmed.ncbi.nlm.nih.gov/24712512/)
5. Ianora A, Boersma M, Casotti R, Fontana A, Harder J, Hoffmann F, et al. *New Trends in Marine Chemical Ecology.* Estuar Coast. 2006; 29: 531–551.
6. Garcia-Altare M, Tartaglione L, Dell'Aversano C, Carnicer O, de la Iglesia P, Forino M, et al. The novel ovatoxin-g and isobaric palytoxin (so far referred to as putative palytoxin) from *Ostreopsis cf. ovata* (NW Mediterranean Sea): structural insights by LC-high resolution MS(n). *Anal Bioanal Chem.* 2015; 407: 1191–204. doi: [10.1007/s00216-014-8338-y](https://doi.org/10.1007/s00216-014-8338-y) PMID: [25492088](https://pubmed.ncbi.nlm.nih.gov/25492088/)
7. Ciminiello P, Dell'Aversano C, Dello Iacovo E, Fattorusso E, Forino M, Grauso L, et al. Complex palytoxin-like profile of *Ostreopsis ovata*. Identification of four new ovatoxins by high-resolution liquid chromatography/mass spectrometry. *Rapid Commun Mass Sp.* 2010; 24: 2735–2744.
8. Ciminiello P, Dell'Aversano C, Dello Iacovo E, Fattorusso E, Forino M, Tartaglione L, et al. Unique toxin profile of a Mediterranean *Ostreopsis cf. ovata* strain: HR LC-MSⁿ characterization of ovatoxin-f, a new palytoxin congener. *Chem Res Toxicol.* 2012; 25: 1243–1252. doi: [10.1021/bx300085e](https://doi.org/10.1021/bx300085e) PMID: [22502872](https://pubmed.ncbi.nlm.nih.gov/22502872/)
9. Tubaro A, Durando P, Del Favero G, Ansaldi F, Icardi G, Deeds JR, et al. Case definitions for human poisonings postulated to palytoxins exposure. *Toxicol.* 2011; 57: 478–495. doi: [10.1016/j.toxicol.2011.01.005](https://doi.org/10.1016/j.toxicol.2011.01.005) PMID: [21255599](https://pubmed.ncbi.nlm.nih.gov/21255599/)
10. Ciminiello P, Dell'Aversano C, Dello Iacovo E, Fattorusso E, Forino M, Tartaglione L, et al. First finding of *Ostreopsis cf. ovata* toxins in marine aerosols. *Environ Sci Technol.* 2014; 48: 3532–3540. doi: [10.1021/es405617d](https://doi.org/10.1021/es405617d) PMID: [24564517](https://pubmed.ncbi.nlm.nih.gov/24564517/)

11. Aligizaki K, Katikou P, Nikolaidis G, Panou A. First episode of shellfish contamination by palytoxin-like compounds from *Ostreopsis* species (Aegean Sea, Greece). *Toxicon*. 2008; 51: 418–427. PMID: [18067938](#)
12. Faimali M, Giussani V, Piazza V, Garaventa F, Corrà C, Asnaghi V, et al. Toxic effects of harmful benthic dinoflagellate *Ostreopsis ovata* on invertebrate and vertebrate marine organisms. *Mar Environ Res*. 2012; 76: 97–107. doi: [10.1016/j.marenvres.2011.09.010](#) PMID: [22000703](#)
13. Di Turi L, Lo Caputo S, Marzano MC, Pastorelli AM, Pompei M, Rositani L, et al. *Ostreopsidaceae* (Dinophyceae) presence along the coastal area of Bari. *Biol Mar Medit*. 2003; 10: 675–678.
14. Vale C, Ares IR. Biochemistry of palytoxins and ostreocins. In: Botana LM, editor. *Phycotoxins, chemistry and biochemistry*. Blackwell Publishing, Ames, IA, USA; 2007. pp. 95–118.
15. Totti C, Accoroni S, Cerino F, Cucchiari E, Romagnoli T. *Ostreopsis ovata* bloom along the Conero Riviera (northern Adriatic Sea): relationships with environmental conditions and substrata. *Harmful Algae*. 2010; 9: 233–239.
16. Vanucci S, Pezzolesi L, Pistocchi R, Ciminiello P, Dell'Aversano C, Dello Iacovo E, et al. Nitrogen and phosphorus limitation effects on cell growth, biovolume, and toxin production in *Ostreopsis* cf. *ovata*. *Harmful Algae*. 2012; 15: 78–90.
17. Redfield AC. On the proportions of organic derivatives in sea water and their relation to the composition of plankton. In: Daniel RJ, editor. *James Johnstone Memorial Volume*. Liverpool University Press, Liverpool, United Kingdom; 1934. pp. 176–192.
18. Redfield AC. The biological control of chemical factors in the environment. *Am Sci*. 1958; 46: 205–221.
19. Vidyarthna NK, Granéli E. Physiological responses of *Ostreopsis ovata* to changes in N and P availability and temperature increase. *Harmful Algae*. 2013;21–22: 54–63.
20. Pezzolesi L, Pistocchi R, Fratangeli F, Dell'Aversano C, Dello Iacovo E, Tartaglione L. Growth dynamics in relation to the production of the main cellular components in the toxic dinoflagellate *Ostreopsis* cf. *ovata*. *Harmful Algae*. 2014; 36: 1–10.
21. Blackford JC, Allen JI, Gilbert FJ. Ecosystem dynamics at six contrasting sites: a generic modelling study. *J Mar Syst*. 2004; 52: 191–215.
22. Guillard RRL. Culture of phytoplankton for feeding marine invertebrates. In: Smith WL, Chanley MH, editors. *Culture of marine invertebrates animals*. Plenum Press, New York; 1975. pp. 26–60.
23. Menzel DW, Corwin N. The measurement of total phosphorus in sea water based on the liberation of organically bound fraction by persulfate oxidation. *Limnol Oceanogr*. 1965; 10: 280–282.
24. Vidyarthna NK, Granéli E. Influence of temperature on growth, toxicity and carbohydrate production of a Japanese *Ostreopsis ovata* strain, a toxic-bloom-forming dinoflagellate. *Aquat Microb Ecol*. 2012; 65: 261–270.
25. Honsell G, Bonifacio A, De Bortoli M, Penna A, Battocchi C, Ciminiello P, et al. New insights on cytological and metabolic features of *Ostreopsis* cf. *ovata* Fukuyo (Dinophyceae): a multidisciplinary approach. *PLoS ONE*. 2013; 8: e57291. doi: [10.1371/journal.pone.0057291](#) PMID: [23460837](#)
26. Geider R, La Roche J. Redfield revisited: variability of C:N:P in marine microalgae and its biochemical basis. *Eur J Phycol*. 2002; 37: 1–17.
27. Ho TY, Quigg A, Finkel ZV, Milligan AJ, Wyman K, Falkowski PG, et al. The elemental composition of some marine phytoplankton. *J Phycol*. 2003; 39: 1145–1159.
28. Goldman JC. On phytoplankton growth rates and particulate C: N: P ratios at low light. *Limnol Oceanogr*. 1986; 31: 1358–1363.
29. John EH, Flynn K J. Growth dynamics and toxicity of *Alexandrium fundyense* (Dinophyceae): the effect of changing N:P supply ratios on internal toxin and nutrient levels. *Eur J Phycol*. 2000; 35: 11–23.
30. Klausmeier CA, Litchman E, Daufresne T, Levin SA. Optimal nitrogen-to-phosphorus stoichiometry of phytoplankton. *Nature*. 2004; 429: 171–174. PMID: [15141209](#)
31. Shibata A, Goto Y, Saito H, Kikuchi T, Toda T, Taguchi S. Comparison of SYBR Green I and SYBR Gold stains for enumerating bacteria and viruses by epifluorescence microscopy. *Aquat Microb Ecol*. 2006; 43: 223–231.
32. Fagerbakke KM, Haldal M, Norland S. Content of carbon, nitrogen, oxygen, sulfur and phosphorus in native aquatic and cultured bacteria. *Aquat Microb Ecol*. 1996; 10: 15–27.
33. Steenbergh AK, Bodelier PLE, Haldal M, Slomp CP, Laanbroek HJ. Does microbial stoichiometry modulate eutrophication of aquatic ecosystems? *Environ Microbiol*. 2013; 15: 1572–1579. doi: [10.1111/1462-2920.12042](#) PMID: [23227825](#)
34. Goldman JC, Caron DA, Dennet MR. Regulation of gross growth efficiency and ammonium regeneration in bacteria by C:N ratio. *Limnol Oceanogr*. 1987; 32: 1239–1252.

35. Ciminiello P, Dell'Aversano C, Dello Iacovo E, Fattorusso E, Forino M, Tartaglione L. LC-MS of palytoxin and its analogues: state of the art and future perspectives. *Toxicon*. 2011; 57: 376–389. doi: [10.1016/j.toxicon.2010.11.002](https://doi.org/10.1016/j.toxicon.2010.11.002) PMID: [21070802](https://pubmed.ncbi.nlm.nih.gov/21070802/)
36. Droop MR. The nutrient status of algal cells in continuous culture. *J Mar Biol Assoc UK*. 1974; 54: 825–855.
37. Geider RJ, MacIntyre HL, Kana TM. Dynamic model of phytoplankton growth and acclimation: responses of the balanced growth rate and the chlorophyll a:carbon ratio to light, nutrient-limitation and temperature. *Mar Ecol Prog Ser*. 1997; 148: 187–200.
38. Pfister LA, Anderson DM. Dinoflagellate reproduction. In: Taylor FJR, editor. *The biology of dinoflagellates*. Blackwell, Oxford, United Kingdom; 1987. pp. 611–648.
39. Polimene L, Allen JI, Zavatarelli M. Model of interactions between dissolved organic carbon and bacteria in marine systems. *Aquat Microb Ecol*. 2006; 43: 127–138.
40. Saltelli A, Ratto M, Andres T, Campolongo M, Cariboni J, Gatelli D, et al. *Global sensitivity analysis. The primer*. John Wiley & Sons Ltd, Chichester, UK; 2008.
41. Pastres R, Ciavatta S. A comparison between the uncertainties in model parameters and in forcing functions: its application to a 3D water-quality model. *Environ Modell Softw*. 2005; 20: 981–989.
42. Ciavatta S, Lovato T, Ratto M, Pastres R. Global uncertainty and sensitivity analysis of a food-web bioaccumulation model. *Environ Toxicol Chem*. 2009; 28: 718–732. doi: [10.1897/08-102R.1](https://doi.org/10.1897/08-102R.1) PMID: [19391679](https://pubmed.ncbi.nlm.nih.gov/19391679/)
43. Saltelli A, Chan K, Scott M. *Sensitivity Analysis. Wiley Series in Probability and Statistics*. New York: John Wiley and Sons; 2000.
44. Hardison DR, Sunda WG, Litaker RW, Shea D, Tester PA. Nitrogen limitation increases brevetoxins in *Karenia brevis* (Dinophyceae): implications for bloom toxicity. *J Phycol*. 2012; 48: 844–858.
45. Hardison DR, Sunda WG, Shea D, Litaker RW. Increased toxicity of *Karenia brevis* during phosphate limited growth: ecological and evolutionary implications. *PLoS ONE*. 2013; 8: e58545. doi: [10.1371/journal.pone.0058545](https://doi.org/10.1371/journal.pone.0058545) PMID: [23554901](https://pubmed.ncbi.nlm.nih.gov/23554901/)
46. Flynn KJ. Do external resource ratios matter? Implications for modelling eutrophication events and controlling harmful algal blooms. *J Mar Sys*. 2010; 83: 170–180.
47. Geider RJ, MacIntyre HL, Kana TM. A dynamic regulatory model of phytoplankton acclimation to light, nutrients, and temperature. *Limnol Oceanogr*. 1998; 43: 679–694.
48. Grzebyk D, Béchemin C, Ward CJ, Vérité C, Codd GA, Maestrini SY. Effects of salinity and two coastal waters on the growth and toxin content of the dinoflagellate *Alexandrium minutum*. *J Plankton Res*. 2003; 25: 1185–1199.
49. Flynn K, Franco JM, Fernández P, Reguera B, Zapata M, Wood G, et al. Changes in toxin content, biomass and pigments of the dinoflagellate *Alexandrium minutum* during nitrogen refeeding and growth into nitrogen and phosphorus stress. *Mar Ecol Prog Ser*. 1994; 111: 99–109.
50. Fiori E, Mazzotti M, Guerrini F, Pistocchi R. Combined effects of the herbicide terbuthylazine and temperature on different flagellates from the Northern Adriatic Sea. *Aquat Toxicol*. 2013; 128–129: 79–90.
51. Falkowski G., Dubinsky Z., Wyman K. Growth-irradiance relationships in phytoplankton. *Limnol Oceanogr*. 1985; 30: 311–321.
52. Burkholder JM, Glibert PM, Skelton HM. Mixotrophy, a major mode of nutrition for harmful algal species in eutrophic waters. *Harmful Algae*. 2008; 8: 77–93.
53. Jeong HJ, Yoo YD, Kim JS, Seong KA, Kang NS, Kim TH. Growth, feeding and ecological roles of the mixotrophic and heterotrophic dinoflagellates in marine planktonic food webs. *Ocean Sci J*. 2010; 45: 65–91.
54. Raven JA. Phagotrophy in phototrophs. *Limnol Oceanogr*. 1997; 42: 198–205.
55. Pistocchi R, Pezzolesi L, Guidi F, Vanucci S, Guerrini F, Pinna A. In: *Proceedings of 16th ICHA conference. Inorganic nutrients uptake and organic phosphorus utilization by *Ostreopsis cf. ovata**. 2014. p. 104.
56. Barone R., Prisinzano A. Peculiarità comportamentale del dinoflagellato *Ostreopsis ovata* Fukuyo (Dinophyceae): la strategia del ragno. 2006; *Nat sicil.*, S. IV, XXX 3–4: 401–418.
57. Faust MA. Mixotrophy in tropical benthic dinoflagellates. In: Reguera B, Blanco J, Fernandez ML, Watt T, editors. *Harmful algae*. Xunta de Galicia and IOC Commission of UNESCO, Paris, France; 1998. pp. 390–393.
58. Vanucci S, Guerrini F, Pezzolesi L, Dell'Aversano C, Ciminiello P, Pistocchi R. Cell growth and toxins' content of *Ostreopsis cf. ovata* in presence and absence of associated bacteria. *Cryptogamie Algol*. 2012; 33: 105–112.

59. Wagner-Döbler I, Ballhausen B, Berger M, Brinkhoff T, et al. The complete genome sequence of the algal symbiont *Dinoroseobacter shibae*: a hitchhiker's guide to life in the sea. *The ISME journal*. 2010; 4: 61–77. doi: [10.1038/ismej.2009.94](https://doi.org/10.1038/ismej.2009.94) PMID: [19741735](https://pubmed.ncbi.nlm.nih.gov/19741735/)
60. Amin SA, Parker MS, Armbrust EV. Interaction between diatoms and bacteria. *Microbiol Mol Biol R*. 2012; 76: 667–686.
61. Bagøien E, Miranda A, Reguera B, Franco JM. Effects of two paralytic shellfish toxin producing dinoflagellates on the pelagic harpacticoid copepod *Euterpina acutifrons*. *Mar Biol*. 1996; 126: 361–369.
62. Waggett RJ, Tester PA, Place AR. Anti-grazing properties of the toxic dinoflagellate *Karlodinium veneficum* during predator—prey interactions with the copepod *Acartia tonsa*. *Mar Ecol Prog Ser*. 2008; 366: 31–42.
63. Irigoien X, Flynn KJ, Harris RP. Phytoplankton blooms: a 'loophole' in microzooplankton grazing impact? *J Plankton Res*. 2005; 27: 313–321.
64. Polimene L, Mitra A, Sailley SF, Ciavatta S, Widdicombe CE, Atkinson A, et al. Decrease in diatom palatability contributes to bloom formation in the Western English Channel. *Prog Oceanogr*. 2015.
65. Accoroni S, Romagnoli T, Pichierri S, Totti C. New insights on the life cycle stages of the toxic benthic dinoflagellate *Ostreopsis cf. ovata*. *Harmful Algae*. 2014; 34: 7–16.
66. Bravo I, Vila M, Casabianca S, Rodriguez F, Rial P, Riobó P, et al. Life cycle stages of the benthic palytoxin-producing dinoflagellate *Ostreopsis cf. ovata* (Dinophyceae). *Harmful Algae*. 2012; 18: 24–34.
67. Adolf JE, Bachvaroff TR, Place AR. Environmental modulation of karlotoxin levels in strains of the cosmopolitan dinoflagellate, *Karlodinium veneficum* (Dinophyceae). *J Phycol*. 2009; 45: 176–192.
68. Johansson N, Granéli E, Yasumoto T, Carlsson P, Legrand C. Toxin production by *Dinophysis acuminata* and *D. acuta* cells grown under nutrient sufficient and deficient conditions. In: Yasumoto T, Oshima Y, Fukuyo Y, editors. *Harmful and toxic algal blooms*. Intergovernmental Oceanographic Commission of UNESCO, Paris, France; 1996. pp. 277–280.
69. Johansson N., Granéli E. Cell density, chemical composition and toxicity of *Chrysochromulina polylepsis* (Haptophyta) in relation to different N:P supply ratios. *Mar Biol*. 1999; 135: 209–217.
70. Tillmann U, Alpermann TL, da Purificação R, Krock B, Cembella A. Intra-population clonal variability in allelochemical potency of the toxigenic dinoflagellate *Alexandrium tamarense*. *Harmful Algae*. 2009; 8: 759–769.
71. Thessen AE, Bowers HA, Stoecker DK. Intra- and interspecies differences in growth and toxicity of *Pseudo-nitzschia* while using different nitrogen sources. *Harmful Algae*. 2009; 8: 792–810.
72. Ciminiello P, Dell'Aversano C, Dello Iacovo E, Fattorusso E, Forino M, Grauso L, et al. Isolation and structure elucidation of ovatoxin-a, the major toxin produced by *Ostreopsis ovata*. *J Am Chem Soc*. 2012; 134: 1869–1875. doi: [10.1021/ja210784u](https://doi.org/10.1021/ja210784u) PMID: [22235929](https://pubmed.ncbi.nlm.nih.gov/22235929/)
73. Selander E, Thor P, Toth G, Pavia H. Copepods induce paralytic shellfish toxin production in marine dinoflagellates. *Proc. R. Soc. B* 2006; 273:1673–1680. doi: [10.1098/rspb.2006.3502](https://doi.org/10.1098/rspb.2006.3502)
74. Senfit-Batch CD, Dam HG, Shumway SE, Wikfors GH. A multi-phylum study of grazer-induced paralytic shellfish toxin production in the dinoflagellate *Alexandrium fundyense*: A new perspective on control of algal toxicity. *Harmful Algae*. 2015; 44:20–31. <http://dx.doi.org/10.1016/j.hal.2015.02.008>